

A possible link among pulsar timing noise intermittency and hidden ultra-compact binaries

B.P. Gong^{1*}, Y.P. Li^{2†}

¹*Department of Physics, Huazhong University of Science and Technology, Wuhan 430074, China,*

²*Department of Astronomy, Xiamen University, Xiamen, 361005, China*

Accepted, Received ;

ABSTRACT

The quasi-periodic feature of 1-10 years exhibited in pulsar timing noise has not been well understood since 1980. The recently demonstrated correlation between timing noise and variation of pulse profile motivates us to further investigate its origins. We suggest that the quasi-periodicity feature of timing noise, with rapid oscillations lying on lower frequency structure, comes from the geodetic precession of an unseen binary system, which induces additional motion of the pulsar spin axis. The resultant change of azimuth and latitude at which the observer's line of sight crosses the emission beam is responsible for the variation of timing noise and pulse profile respectively. The first numerical simulation to both timing noise and pulse profile variation are thus performed, from which the orbital periods of these pulsars are of 1-35 minutes. Considering the existence of the ultracompact binary white dwarf of orbital period of 5.4 minute, HM Cancri, such orbital periods of pulsar binaries are not strange. The change of latitude of the magnetic moment exceeding the range of emission beam of a pulsar results in the intermittency, which explains the behavior of PSR B1931+24. Therefore, it provides not only a mechanism of the quasi-periodic feature displayed on some "singular" pulsars, like timing noise, variation of pulse profile and intermittency; but also a new approach of searching ultra-compact binaries, possibly pulsar-black hole binary systems.

Key words:

Stars: evolution , Pulsars: individual(PSR B1540–06,PSR B1828–11,PSR B1931+24)

1 INTRODUCTION

Pulsar timing noise is the discrepancy between pulsar arrival times at an observatory and times predicted from a spin down model, containing the rotational frequency and its derivative. Such low-frequency structures previously observed in pulsar data sets have been explained by random processes (Cordes et al. 1980; Lyne et al. 2000), unmodelled planetary companions (Cordes 1993) or free-precession (Stairs et al. 2000). However, these models predict either random or exact periodic timing delay, which cannot well account for the quasi-periodic feature revealed, i.e., in the large investigation of pulsar rotation properties (Hobbs et al. 2010).

Lyne et al. (2010) reported the correlation of timing noise with changes in the pulse shape in six pulsars. And the link among mode changing (Wang et al. 2007), nulling,

intermittency, pulse-shape variability, and timing noise is addressed. These phenomena are attributed to the change in the pulsar's magnetosphere (Lyne et al. 2010).

This paper shows that the geodetic precession induced motion of pulsar spin axis can change both the latitude and azimuth of the magnetic moment of the pulsar, which mimics the magnetosphere change, and hence well account for the quasi-periodic structure and its correlated phenomena.

In the absence of spin precession, the magnetic moment of the pulsar, μ , with a misalignment angle, α , relative to the spin axis, rotates around a fixed axis (Radhakrishnan & Cook 1969). The observed pulsed emission occurs when the pulsar beam sweeps past the line of sight, in the case of dipole magnetic field, as shown in Fig. 1.

If a pulsar is in orbit with a rotating companion star, then the two spinning tops are in the gravitation field of each other, and both the spin axes will precess around the common orbital angular momentum vector. This is the so-called geodetic precession. The precession of a pulsar spin

* E-mail: bpgong@mail.hust.edu.cn

† E-mail: liyp@stu.xmu.edu.cn

axis will cause additional motion of the magnetic moment, μ , owing to a fixed, α , the misalignment angle between the spin axis and μ . Consequently, both the azimuth and latitude at which the observer's line of sight crosses the beam change, which in turn leads to quasi-periodic timing delay and variation in pulse profile respectively. However, these pulsars with significant timing noise are usually identified as isolated pulsars instead of binary ones. This problem can be explained by three reasons.

Firstly, the current limit on binary search is 90 minutes for radio pulsars, and 10 minutes for X-ray pulsars. In other words, pulsars with orbital period shorter than these thresholds have not been detected. But from the stand of evolution of binary pulsars, it is difficult to understand why binary pulsars with orbital period less than 90 minutes or 10 minutes cannot exist. Obviously, the limit is of technique rather than true existence. Therefore, it is possible that some of these isolated pulsars with significant timing noise are binary pulsars beyond the threshold of binary detection.

Secondly, e.g., PSR 1828-11 has several 8-min continuous time series observed by Parkes telescope (R.N. Manchester, private communication), but none of them cover a full proposed orbital period of ~ 20 min. Thus, orbital modulation on the timing of PSR 1828-11 has never been observed in over a complete orbital period, although it has been observed for years.

Thirdly, the short-term effect of a binary system, i.e., the time delay corresponding to the propagation time of pulsar emission during its orbital motion, the Römer delay, depends on the amplitude of semi-major axis of a binary, a . Apparently a small a leads to low signal to noise ratio in time of arrival. Moreover, ultra-compact binaries correspond to rapid orbital motion which prevents from having good quality profile (to discern orbital modulation) in such short orbital bins.

Whereas, the geodetic precession induced additional time delay is a long-term effect (usually lasts a few orders of magnitude longer than that of the short-term effect), the amplitude of which can be large in the case of small a . As a result, the orbital effect of binary pulsars with small a is difficult to detect. In contrast, the corresponding long-term effect is still easy to find. Therefore, such pulsars could be identified as singular pulsars with strong timing noise (Gong 2005, 2006).

How the geodetic precession invokes the quasi-periodic change of timing noise and pulse profile? In the gravitational two-body system, the geodetic precession makes one body precess in the gravitational field of the other, which influences pulsar timing in two ways.

The first one is the spin vector of one body precesses around the orbital angular momentum vector, the precession velocity of which is given by the two-body equation (Barker & O'Connell 1975),

$$\dot{\mathbf{\Omega}}_1 = \frac{L(4 + 3m_2/m_1)}{2r^3} \hat{\mathbf{L}} = T_\odot^{2/3} \left(\frac{2\pi}{P_b^*}\right)^{3/5} \times \frac{M_r(4 + 3M_r)}{2(1 + M_r)^{4/3}} \hat{\mathbf{L}}(1)$$

where L and $\hat{\mathbf{L}}$, are magnitude and unit vector of the orbital angular momentum, m_1 and m_2 are masses of the two bodies, and r the separation between them; $M_r \equiv m_1/m_2$, $T_\odot \equiv GM_\odot/c^3 = 4.925490947\mu\text{s}$ and $P_b^* \equiv P_b(1 - e^2)^{3/5}/(m_1^*)^{2/5}$ (where $m_1^* \equiv m_1/M_\odot$, P_b and e are orbital period and eccentricity respectively). Notice that in Eq.(1)

the expression without T_\odot is the original two-body equation (Barker & O'Connell 1975), and the one with T_\odot is rewritten for the convenience of numerical calculation. Here after the observed pulsar is labeled by subscript 1, and its companion star by 2.

As shown in Fig.(1), the geodetic precession can change the orientation of spin axis, and thus affects the azimuth and the latitude at which the observer's line of sight crosses the beam. Such an additional motion of a pulsar spin axis can be analyzed equivalently by assuming a constant pulsar spin angular momentum vector, but a varying line of sight (LOS), in a reference frame defined by the spin angular momentum vector of the pulsar, \mathbf{S}_1 , (\mathbf{i}' , \mathbf{j}' , \mathbf{k}').

Another useful reference frame is defined by the angular momentum vector, \mathbf{L} , (\mathbf{i} , \mathbf{j} , \mathbf{k}), in which the direction toward the observer, \mathbf{n} , is in the plane defined by the unit vectors, \mathbf{i} and \mathbf{k} , $\mathbf{n} = (\sin i, 0, \cos i)$. Transforming from the reference frame defined by \mathbf{L} , to the reference frame defined by \mathbf{S}_1 , the LOS is changed from unit vector, \mathbf{n} to \mathbf{n}' , which is read (Konacki et al. 2003),

$$\mathbf{n}' = R(-\lambda)R(\Psi)\mathbf{n}, \quad (2)$$

where \mathbf{n} first rotates around the axis \mathbf{k} by the angle, Ψ , then around the axis \mathbf{j} by angle, $-\lambda$.

A pulse is identified when the magnetic moment, μ , crosses the plane defined by the vectors, \mathbf{n}' , and \mathbf{S}_1 and, at the same time, the angle between \mathbf{n}' , and μ does not exceed the opening semi-angle ρ , as shown in Fig. 1. Obviously, the direction toward the observer \mathbf{n}' changes with the precession phase Ψ , which can make a pulse arrive advanced or retarded than that of a fixed \mathbf{n}' . This effect can be quantified by the azimuthal angle of \mathbf{n}' (Konacki et al. 2003),

$$\tan \Theta(t) = n'_y(t)/n'_x(t) \quad (3)$$

Apparently, a two-body system with a single spin precessing as Eq.(1) will result in the timing effect of Eq.(3), which predicts a periodic timing effect similar to the free precession.

Here is the second way that the geodetic precession influences pulsar timing. A two-body system with spin can cause an additional perturbation to the classical two-body system without spin, and hence, all six orbital elements of a binary vary, including ω and Ω , the precession of periastron and the longitude of precession of the orbital plane respectively (Smarr & Blandford 1976). However, the contribution of ω and Ω to Römer delay depends on the projected semi-major axis, x (Lai et al. 1995). On the contrary, the precession induced long-term azimuthal time delay, as shown in Eq.(2) and Eq.(3), is not directly related with x , which can be significant in the case of small x .

The arrangement of this paper is as follows. Section 2 shows the long-term additional time delay and change of pulse width caused by Ω , the precession speed of the orbital angular momentum vector, \mathbf{L} , around the total angular momentum, \mathbf{J} . Section 3 applies the model to three pulsars, fitting their quasi-periodicity timing noise, and simulating the corresponding variation of pulsar profile width and intermittency for the first time. The discussion and conclusion of results are presented in the final Section.

2 LONG-TERM BINARY EFFECT ON PULSAR TIMING

When $\dot{\Omega}$, the precession of the orbital angular momentum vector, \mathbf{L} , around the total angular momentum, \mathbf{J} , which has been ignored by Eq.(2) and Eq.(3), is considered, the LOS should be transformed as,

$$\mathbf{n}' = R(-\lambda_1)R(\Psi)R(\lambda_{LJ})R(\Omega)\mathbf{n}_0, \quad (4)$$

where λ_{LJ} is the misalignment angle between \mathbf{L} and \mathbf{J} , and $\mathbf{n}_0 = (0, \sin I, \cos I)$ is the unit vector of LOS defined in the reference frame $(\mathbf{i}_0, \mathbf{j}_0, \mathbf{k}_0)$ with \mathbf{k}_0 aligned with \mathbf{J} , as shown in Fig. 1. Thus, putting the components $n'_x(t)$ and $n'_y(t)$ obtained from Eq.(4) into Eq.(3), the time delay including to the precession of orbital plane can be obtained.

Note that Eq.(4) has one more frame transformation than that of Eq.(2), which is realized by the rotation of $R(\lambda_{LJ})$ and $R(\Omega)$. In Eq.(4), the LOS, \mathbf{n}_0 , is firstly transformed to the reference frame with \mathbf{k} aligned with \mathbf{L} . And then it transforms from the frame defined by \mathbf{L} to the frame defined by the spin angular momentum, \mathbf{S}_1 , as that in Eq.(2).

The conservation of the total angular momentum, \mathbf{J} , must be held during the precession of the two bodies, which requires that \mathbf{L} and \mathbf{S} ($\mathbf{S} = \mathbf{S}_1 + \mathbf{S}_2$) be on the opposite side of \mathbf{J} at any moment (Smarr & Blandford 1976; Hamilton & Sarazin 1982). In other words, the plane determined by the three vectors, \mathbf{J} , \mathbf{S} and \mathbf{L} rotates around the vector \mathbf{J} instantaneously. In the study of the modulation of the gravitational wave by Spin-Orbit coupling effect on merging binaries, the orbital precession velocity satisfying the conservation of the total angular momentum, and the triangle constraint have been studied extensively (Apostolatos et al. 1994; Kidder 1995).

Apparently, the precession of the two spins, \mathbf{S}_1 and \mathbf{S}_2 , can change the total spin angular momentum vector, \mathbf{S} , and hence varies λ_{LJ} through the triangle formed by \mathbf{S} , \mathbf{L} and \mathbf{J} . Then, λ_{LJ} can simply be obtained by, $\lambda_{LJ} = \sin^{-1}(\sqrt{S_x^2 + S_y^2}/L)$, as shown in Fig. 1.

Moreover, Ω can be easily obtained by the precession phase of the two spins, $\Omega = \tan^{-1}(-S_x/S_y)$, where $S_x = S_1 \sin \lambda_1 \cos \eta_1 + S_2 \sin \lambda_2 \cos \eta_2$ and $S_y = S_1 \sin \lambda_1 \sin \eta_1 + S_2 \sin \lambda_2 \sin \eta_2$ in which $\eta_1 = \Omega_1 t + \eta_{10}$, $\eta_2 = \Omega_2 t + \eta_{20}$ (where η_{10} and η_{20} are initial phases).

Therefore, just starting from the very basic principles, the conservation of the total angular momentum, \mathbf{J} , the variation of λ_{LJ} and Ω required in Eq.(4) can be obtained respectively.

Putting the precession phase of the pulsar (in the reference frame defined by \mathbf{L}), $\Psi = \eta_1 - \Omega$, and λ_{1L} the misalignment angle between the spin angular momentum, \mathbf{S}_1 , and \mathbf{L} , into Eq.(4), the additional time delay can be calculated, which predicts a quasi-periodic variation. Notice that the polar angle of \mathbf{S}_1 and \mathbf{S}_2 with respect to \mathbf{L} is treated as equal to λ_1 and λ_2 , the misalignment angles with \mathbf{J} respectively, which are good approximations in the case of $\lambda_{LJ} \ll 1$.

Besides the azimuthal effect, the geodetic precession can induce latitude effect and hence vary the pulse profile as well, as shown in Fig.1. The impact angle between the beam axis and LOS is given, $\beta = \cos^{-1} n'_z - \alpha$, from which the pulse width can be obtained (Lyne & Manchester 1988),

$$\mathcal{W}(t) = 2 \cos^{-1} \left[\frac{\cos \rho - \cos \alpha \cos(\alpha + \beta)}{\sin \alpha \sin(\alpha + \beta)} \right] \quad (5)$$

Notice that the width variation of Eq.(5), is derived under the assumption of circular beam, the geometry of which needs only two parameters, half-opening angle of the beam, ρ and magnetic inclination angle, α , as shown in Fig. 1.

3 APPLICATION TO THREE PULSARS

Having simple modification to the geodetic precession induced timing effect, the new model is applied to three pulsars (Lyne et al. 2010; Kramer et al. 2006). In the fitting of timing residuals, we focus on whether the very basic features predicted by the model fit the quasi-periodic characteristics exhibited in these pulsars.

Monte Carlo method is performed to search the best combination of parameters that make Eq.(4) fit the timing noise of the three pulsars, the best fit parameters are given in Table 1. In the fitting of a timing noise structure, such as Fig.2-4, 10 parameters are used, three binary parameters, P_b^* , M_r , I ; and six parameters for the spin angular momenta of the two bodies, \mathbf{S}_1 and \mathbf{S}_2 , which are their magnitude (S_1, S_2), misalignment angle with the total angular momentum (λ_1, λ_2), precession phases (η_1, η_2), as well as the parameter, ϕ_0 , representing the initial phase of $\Theta(t)$ in Eq.(3), as shown in Table 1.

Although the timing noise displayed in the three pulsars appear different, the relatively rapid oscillations lie on lower-frequency structures is common for all of them, which differs only in relative amplitude of oscillations and in the time scale of quasi-periods.

Among the three pulsars with significant timing noise, two pulsars, PSR B1540-06 and PSR B1828-11 have observations both in timing residual and variation of pulse width (Lyne et al. 2010). In our model, these two effects are fitted by Eq.(4) and Eq.(5) respectively.

As shown in Fig.(2) and Table 1, the fitting of both the timing residual and the variation of pulse width of PSR B1540-06 give two solutions, the mass ratio of which are $M_r = 2.63$ and $M_r = 0.51$ respectively as shown in Table 1. This means companion mass of $3.7M_\odot$ and $0.7M_\odot$ respectively, in the case of pulsar mass of $m_1 = 1.4M_\odot$. As shown in Table 1, an orbital period of 35 minutes and companion mass of $3.7M_\odot$ suggests a black hole companion to the binary, well this solution is limited by the large projected semi-axis, x predicted.

The periodicities of 250, 500 and 1000 days have been reported in the rotation rate and pulse shape of PSR B1828-11 (Stairs et al. 2000). These periodicities have been interpreted as being caused by free precession of this pulsar, even though it had been argued that this was not possible in the presence of the superfluid component believed to exist inside neutron stars (Lyne et al. 2010). Apparently, the geodetic precession induced timing and profile variation avoids this difficulty automatically.

The fitting of timing residual and pulse profile variation of PSR B1828-11 also gives two numerical solutions. One solution corresponds to precession periods of $2\pi/\dot{\Omega}_1 = 503d$ and $2\pi/\dot{\Omega}_2 = 592d$ respectively, which accounts for the $\sim 500d$ period shown in Fig.(3). The discrepancy between them corresponds to a period of 3000d which is responsible

for the low-frequency structure displayed in Fig.(3). And the ~ 250 d period can be explained by the period $2\pi/(\dot{\Omega}_1 + \dot{\Omega}_2)$.

The discrepancy between the observed and predicted variation of pulse width displayed in PSR B1540-06 and PSR B1828-11 is mainly due to the assumption of a circular emission beam.

PSR B1931+24 behaves as an ordinary isolated radio pulsar for 5 to 20 days long and switches off for the next 25 to 35 days. Such on and off repeat quasi-periodically. Moreover, it spins down 50% faster when it is on than when it is off. These two unrelated phenomena can be interpreted by the geodetic precession too. As shown in Fig.(4), the timing residual of PSR B1931+24 can also be fitted by the rapid and slow oscillation of quasi-period of 7d and 45d respectively, which correspond to the precession period of the two bodies respectively. Although there are much fewer observational timing residual data points than the other two pulsars, the correlation of timing residual with the on and off states, as shown in Fig.(4), imposes strong constraints on the fitting parameters. The phase discrepancy between timing residual and the on and off states is likely due to the assumption of circular emission beam.

The rapid precession of the spin axis of PSR B1931+24 suggests that it is in a binary pulsar system with period of $\simeq 1$ minute as shown in Table 1. Furthermore, the fitting of the timing residual of PSR B1931+24, as shown in Fig.(4), automatically explains the spin down 50% faster when it is on than when it is off occurred on this pulsar.

The quasi-period of 40d corresponds to so large a variation in misalignment angle between the LOS and the pulsar spin axis that can make the pulsar emission beam outside the LOS. Thus explains the on-off state and hence the intermittency exhibited in this pulsar.

Comparatively, in the other two pulsars, the amplitude of change of β as shown in Fig 1, is not sufficient to move the emission beam out off LOS, although the geodetic precession varies both the timing residual and pulse profile.

4 DISCUSSIONS AND CONCLUSIONS

The first numerical simulation to both timing noise and pulse profile variation are performed, from which the orbital periods of these pulsars are of 1-35 minutes. The quasi-periodicity feature of timing noise, with rapid oscillations lying on lower frequency structure, is well explained in the context of the geodetic precession of an unseen binary system, which induces additional motion of the pulsar spin axis.

Timing noise without such a character, e.g., PSR B0954+08, PSR B0642-03, PSR B1822-09 and PSR B0950+08 (Lyne et al. 2010), cannot be fitted by our model. In other words, the timing noise of these pulsars may have other origins.

As shown in Fig.2-4, it clearly shows that the geodetic precession induced timing effect tends to be more regular, while the true timing noise appears more irregular. Such a deviation may have three reasons. (a) The timing residual like Fig.(3) is obtained by fitting the time of arrival by the rotation equation with parameters, ν , and $\dot{\nu}$ (or $\ddot{\nu}$). The values of these parameters can change the shape of the timing residual. (b) Throughout the fitting, we assume circular emission beam, while the actually beam can be non-circular,

which can also lead to irregularities in both timing residual and pulse profile change. (c) There can be other effects like the quadruple moment in the companion star. Due to more parameters and assumptions would be introduced to account for such issues, we leave it in the future investigations.

As shown in Table 1 and the pulsar mass range discussed above, a typical companion mass of $0.25\text{--}0.34M_\odot$, corresponds to the Roche lobe radius of the companion star, R_2 ,

$$R_2 = 0.462a\left(\frac{M_2}{M_1 + M_2}\right)^{1/3} \simeq 3 \times 10^9(\text{cm}), \quad (6)$$

where the semi-major axis of the binary, a , is $a = 1.6 \times 10^{10}\text{cm}$ (Notice that small $a_p \sim 10^7\text{cm}$ is due to the nearly face one orbital inclination and the small mass ratio, m_2/m_1). The Roche lobe radius of Eq.(6) is not much larger than the typical radius of White dwarf (WD) star of $\sim 1 \times 10^9\text{cm}$. Thus, the possibility of a WD as companion star cannot be excluded. Although more likely candidate would be a strange star (Dey et al. 1998), a quark star (Xu 2003) or even a black hole.

The fitting parameters of Table 1 indicates that the orbital inclination angle, $i \simeq I$, influences the amplitude of the predicted timing residual. Whereas, the semi-major axis of a binary, a , can influence the precession velocity but not the amplitude of predicted timing residual. For a binary with a precession period of a few years, the typical semi-major axis, a , is of $\sim 10^{10}\text{cm}$, and with a small i , the projected semi-major axis, x , can be a few ms. If such pulsars are observed in the single pulse mode at time scale of several or tens of the predicted orbital period as shown in Table 1, their ultra-compact binary nature could be revealed.

The first numerical simulation to the timing residual and its correlated phenomena given by this paper provides an extremely simple scenario to the link among the timing noise, pulse-shape variability and intermittency. The binary assumption appears strange. However, it corresponds to acceptable companion stars and the absence of binary detection is also reasonable. The model can be tested by the comparison between the predicted timing residual, as shown in Fig.2-4 and the observed ones in the near future. And the binary parameters predicted in Table 1 can also be directly tested by timing series of time scale longer or much longer than the predicted orbital periods. E.g., PSR 1828-11 has several 8-min continuous time series observed by Parkes telescope, but none of them cover a full proposed orbital period, ~ 20 min. A future continuous single pulse observation of time scale several orbital periods or a few hours is expected in order to test the predicted binary nature.

This actually proposes a new way of binary searching, which estimates the binary parameters of a candidate pulsar through fitting of its timing noise, and then test the predicted binary parameters via timing series of appropriate time scale. The current threshold of orbital period of 90min of radio binary pulsars could be broken by this approach. And pulsar black hole binary system may be found by this method.

REFERENCES

- Apostolatos, T.A., Cutler, C., Sussman, J.J. & Thorne, K.S. 1994, Phys. Rev. D, 49, 6274
- Barker, B.M. & O'Connell, R.F. 1975, Phys. Rev. D, 12, 329
- Cordes, J. M. & Helfand, D. J. 1980, ApJ, 239, 640
- Cordes, J.M. 1993, in Planets around Pulsars, Astron. Soc. Pac. Conf., ed. Philips, J.A., Thorsett, S.E. & Kulkarni, S.R., 36, 43
- Dey, M., Bombaci, I., Dey, J., Ray, S. & Samanta, B. C. 1998, Physics Letters B, 438, 123
- Gong, B.P., 2005, Phys. Rev. Lett, 95, 261101
- Gong, B.P., 2006, ChJAS, 2006, 6b, 273G
- Hamilton, A.J.S. & Sarazin, G.L. 1982, Mon. Not. R. Astron. Soc., 198, 59
- Hobbs, G., Lyne, A. G. & Kramer, M. 2010, Mon. Not. R. Astron. Soc., 402, 1027
- Kidder, L.E., 1995, Phys. Rev. D, 52, 821
- Konacki, M., Wolszczan, A. & Stairs, I. H. 2003, ApJ, 589, 495
- Kramer, M., Lyne, A. G., O'Brien, J. T., Jordan, C. A. & Lorimer, D. R. 2006, Science, 312, 549
- Lai, D., Bildsten, L. & Kaspi, V.M. 1995, ApJ, 452, 819L
- Lyne, A. G. & Manchester, R. N. 1988, Mon. Not. R. Astron. Soc., 234, 477
- Lyne, A. G., Shemar, S. L. & Smith, F. G. 2000, Mon. Not. R. Astron. Soc., 315, 534
- Lyne, A. G., Hobbs, G., Kramer, M., Stairs, I. & Stappers, B. 2010, Science 329, 408
- Manchester, R. N. et al. 2010, ApJ, 710, 1694
- Provencal, J. L., Shipman, H. L., Hog, E., & Thejll, P. 1998, ApJ, 494, 759
- Radhakrishnan V. & Cook, D.J. 1969, Astrophys. Lett., 3, 226
- Rankin, J. M., Rodriguez, C. & Wright, G. A. E. 2006, Mon. Not. R. Astron. Soc., 370, 673
- Smarr, L.L. & Blandford, R. 1976, ApJ, 207, 574
- Stairs, I.H., Lyne, A.G. & Shemar, S.L. 2000, Nature, 406, 484
- Shabanova, T. V. 2000, ApJ, 721, 251
- Kiziltan, Bulent, Kottas, Athanasios, Thorsett, Stephen E. 2010, , arXiv1011.4291K
- Wang, N., Manchester, R.N. & Johnston, S. 2007, Mon. Not. R. Astron. Soc. 377, 1383
- Xu, R.X. 2003, ApJ, 596, L59

APPENDIX A: DETAILED ROTATION MATRIXES

The four rotation matrixes are expressed as follows:

$$\begin{aligned}
 R(\Omega) &= \begin{pmatrix} \cos \Omega & \sin \Omega & 0 \\ -\sin \Omega & \cos \Omega & 0 \\ 0 & 0 & 1 \end{pmatrix}, R(\lambda_{LJ}) = \begin{pmatrix} 1 & 0 & 0 \\ 0 & \cos \lambda_{LJ} & \sin \lambda_{LJ} \\ 0 & -\sin \lambda_{LJ} & \cos \lambda_{LJ} \end{pmatrix} \\
 R(\Psi) &= \begin{pmatrix} \cos \Psi & \sin \Psi & 0 \\ -\sin \Psi & \cos \Psi & 0 \\ 0 & 0 & 1 \end{pmatrix}, R(-\lambda_1) = \begin{pmatrix} \cos \lambda_1 & 0 & -\sin \lambda_1 \\ 0 & 1 & 0 \\ \sin \lambda_1 & 0 & \cos \lambda_1 \end{pmatrix}.
 \end{aligned}$$

then expanding Eq.(4), the three components of \mathbf{n}' can be written as:

$$n'_x = \cos I (-\cos \lambda_{LJ} \sin \lambda_1 + \cos \lambda_1 \sin \Psi \sin \lambda_{LJ}) + \sin I$$

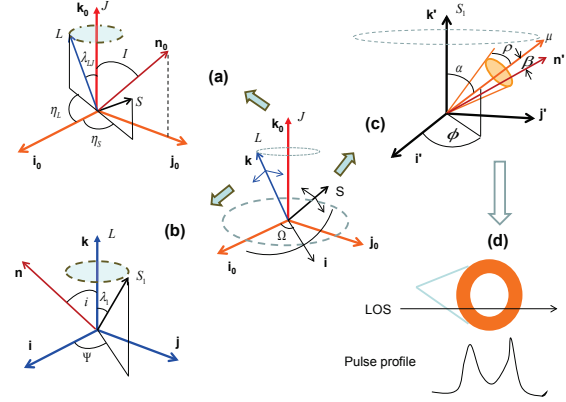


Figure 1. Definition of the angles and three coordinate systems. In the case of $\lambda_{LJ} \ll 1$, which can always be satisfied in our calculation, the approximation, $\Psi = \eta_1 - \Omega$ and $\lambda_{1L} = \lambda_1$ are adopted, where λ_{1L} and λ_1 are the misalignment angle between S_1 and L , as well as S_1 and J respectively.

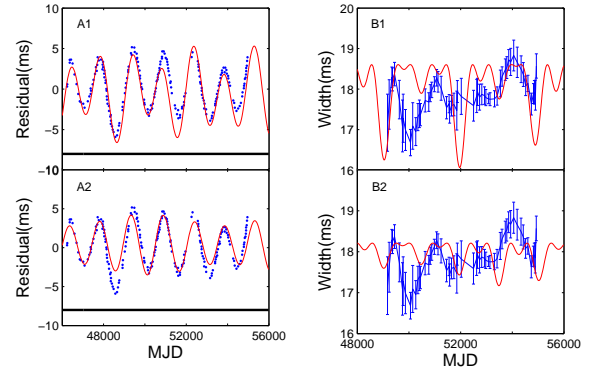


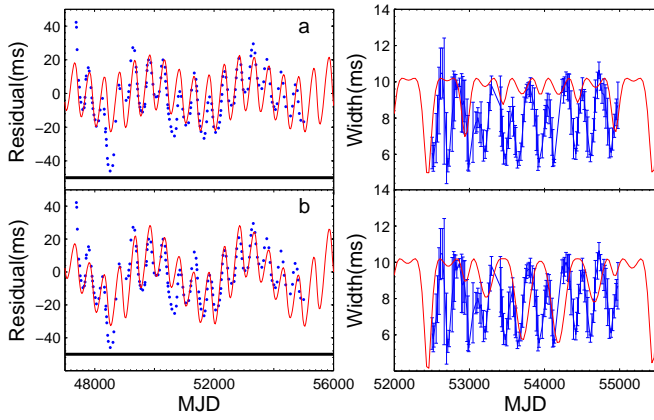
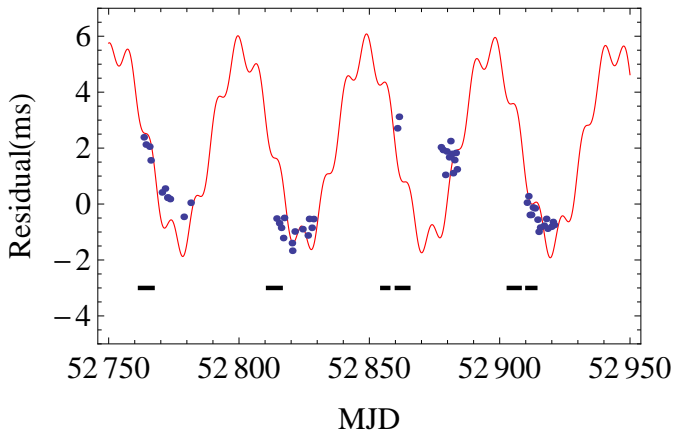
Figure 2. The observed (dotted) and fitted (solid) timing residual and pulse width variation for PSR B1540-06. The upper panels, A1 and B1, show the fitted timing residual and variation of pulse width corresponding to the solution with large mass ratio in Table 1. And the bottom panels, A2 and B2, correspond to that of small mass ratio in Table 1. The horizontal line indicates that this pulsar is always at on-state.

$$\begin{aligned}
 &(\cos \Omega (\cos \lambda_1 \cos \lambda_{LJ} \sin \Psi + \sin \lambda_1 \sin \lambda_{LJ}) + \cos \Psi \cos \lambda_1 \sin \Omega) \\
 &n'_y = \cos I \cos \Psi \sin \lambda_{LJ} + \sin I (\cos \Psi \cos \lambda_{LJ} \cos \Omega - \sin \Psi \sin \Omega) \\
 &n'_z = \cos I (\cos \lambda_1 \cos \lambda_{LJ} + \sin \Psi \sin \lambda_1 \sin \lambda_{LJ}) + \sin I \\
 &(\cos \Omega (\cos \lambda_{LJ} \sin \Psi \sin \lambda_1 - \cos \lambda_1 \sin \lambda_{LJ}) + \cos \Psi \sin \lambda_1 \sin \Omega)
 \end{aligned} \tag{A1}$$

Table 1. The fitting parameters for three pulsars

PSR	rms	$P_b^*(0.01, 2)$	$M_r(0.01, 3)$	$I(0, \pi)$	$c_1(0.0001, 0.01)$	$c_2(0.001, 0.5)$	$\eta_{10}(0, 2\pi)$	$\eta_{20}(0, 2\pi)$	$\lambda_1(0, \pi)$	$\lambda_2(0, \pi)$	$\phi_0(0, 2\pi)$	$\alpha(0, \pi)$	$\rho(0, 30^\circ)$
B1540-06	1.4	0.59	2.63	3.10	0.0018	0.026	4.25	3.56	1.25	2.51	0.0052	1.88	7.5°
	1.3	0.28	0.51	3.12	0.0096	0.063	0.78	4.92	0.59	3.08	-0.0036	2.54	4.3°
B1828-11	13.4	0.22	1.21	2.97	0.0001	0.08	3.71	3.94	0.82	0.94	0.05	2.31	14.4°
	10.4	0.19	0.11	3.09	0.0086	0.055	1.39	2.05	0.24	1.44	0.036	2.90	7.0°
B1931+24	1.3	0.016	0.12	3.12	0.00010	0.0057	5.18	1.48	1.68	0.87	-0.016	1.26	10.0°

The magnetic inclination angle α and half opening angle of emission beam, ρ are obtained through fitting of pulse profile variation or on-off states. All angels, except for ρ , are in radian. P_b is in hour, $M_r \equiv m_1/m_2$; and the spin angular momenta, $c_1 = S_1/L$ and $c_2 = S_2/L$ are dimensionless. ϕ_0 is the initial phase for $\Theta(t)$. The range in the parenthesis followed each parameter indicates the searching parameters space for the fitting process. The root mean square(rms) of fitting is given by $\sqrt{\sum_{j=1}^N (y'_j - y_j)^2 / N'}$, where $N' (= N - 10 - 1)$ is the degree of freedom, y'_j and y_j are the fitted and observed timing residual, respectively.

**Figure 3.** same as Fig.(2) but for PSR B1828-11.**Figure 4.** The observed and fitted timing residual for PSR B1931+24. The dots are the observed timing residual and the solid curve represents the fitted one. The horizontal lines represent the on states of the pulsar predicted by the model.